THE JOURNAL OF PHYSICAL CHEMISTRY A

Article

pubs.acs.org/JPCA

"Watching" the Dark State in Ultrafast Nonadiabatic Photoisomerization Process of a Light-Driven Molecular Rotary Motor

Xiaojuan Pang,[†] Xueyan Cui,[†] Deping Hu,[‡] Chenwei Jiang,*[,†] Di Zhao,[†] Zhenggang Lan,*[,‡] and Fuli Li[†]

[†]Key Laboratory for Quantum Information and Quantum Optoelectronic Devices, Shaanxi, and Department of Applied Physics, Xi'an Jiaotong University, Xi'an 710049, China

[‡]Qingdao Institute of Bioenergy and Bioprocess Technology, Chinese Academy of Sciences, 189 Songling Road, Qingdao, 266101 Shandong China

ABSTRACT: Photoisomerization dynamics of a light-driven molecular rotary motor, 9-(2-methyl-2,3-dihydro-1*H*-cyclopenta[*a*]naphthalen-1-ylidene)-9*H*-fluorene, is investigated with trajectory surface-hopping dynamics at the semiempirical OM2/MRCI level. The rapid population decay of the S_1 excited state for the M isomer is observed, with two different decay time scales (500 fs and 1.0 ps). By weighting the contributions of fast and slow decay trajectories, the averaged lifetime of the S_1 excited state is about 710 fs. The calculated quantum yield of the M-to-P photoisomerization of this molecular rotary motor is about 59.9%. After the $S_0 \rightarrow S_1$ excitation, the dynamical process of electronic decay is followed by twisting about the central C=C double bond and the motion of pyramidalization at the carbon atom of the stator−axle linkage. Although two S_0/S_1 minimum-energy conical intersections are obtained at the OM2/MRCI level, only one conical intersection is found to be responsible for the nonadiabatic dynamics. The existence of "dark state" in the molecular rotary motor is confirmed through the simulated time-resolved fluorescence emission spectrum. Both quenching and red shift of fluorescence emission spectrum observed by Conyard et al. [Conyard, J.; Addison, K.; Heisler, I. A.; Cnossen, A.; Browne, W. R.; Feringa, B. L.; Meech, S. R. *Nat. Chem.* **2012**, *4*, 547−551; Conyard, J.; Conssen, A.; Browne, W. R.; Feringa, B. L.; Meech, S. R. *J. Am. Chem. Soc.* **2014**, *136*, 9692−9700] are well understood. We find that this "dark state" in the molecular rotary motor is not a new electronic state, but the "dark region" with low oscillator strength on the initial S_1 state.

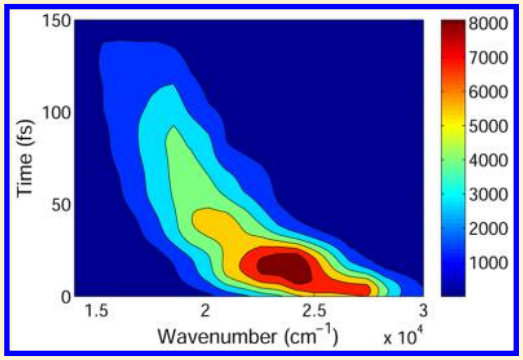

I. INTRODUCTION

Light-driven molecular rotary motors, as one kind of molecular machine to supply energy by converting external light energy to the designed mechanical energy, due to their advantages of cleanliness and ease of control, have been chosen as eligible candidates for an artificial motor[1−3] compared to other motors such as electrically,[4−6] chemically,[7,8] and Brownian[9,10] driven motors. More and more attention has been focused on light-driven molecular rotary motors both experimentally[1,11−28,40−42] and theoretically[29−39,42] during the past two decades.

Light-driven molecular rotary motors based on the chiral crowded alkene designed by Feringa and co-workers[1,20,21] represent a group of promising molecular machines at nanoscale by means of rotating a flexible rotor part relative to a stator. A complete cycle of these molecular rotary motors contains either two steps of photoisomerization combined with two steps of thermal helix inversion[20,21,28] or just two steps of photoisomerization.[28,29,38] To achieve the consecutiveness and unidirectionality of a molecular rotary motor, the periodic repetition mechanism based on molecular structure rearrangement plays an important role in chiral overcrowded alkenes.[1,19−21]

Whether two-step or four-step types of molecular motors, increasing the operational efficiency of unidirectional rotation is a key challenge. Considerable progress[22−27,30−33] has been made in optimizing the frequency and efficiency of ground sate rotation both theoretically and experimentally in the past two decades. Through optimized chemical synthesis, the order of magnitude of rotation frequencies has been increased to megahertz, which is able to match the process of photoisomerization steps.[26,27]

To the best of our knowledge, less attention has been focused on the excited state process in light-driven molecular rotary motors, which may become the bottleneck for improving the operational efficiency. On the theory side, with classical molecular dynamics simulation using the OPLS force field, Kazaryan et al.[34] studied the photoisomerization step of a prototypical fluorene-based molecular rotary motor, 9-(2,4,7-trimethyl-2,3-dihydro-1*H*-inden-1-ylidene)-9*H*-fluorene, which was synthesized by Feringa's group. The excited state lifetimes and photostationary state ratio are reconfirmed by their later

Received: December 6, 2016
Revised: January 15, 2017
Published: January 19, 2017

DOI: 10.1021/acs.jpca.6b12253
J. Phys. Chem. A 2017, 121, 1240−1249

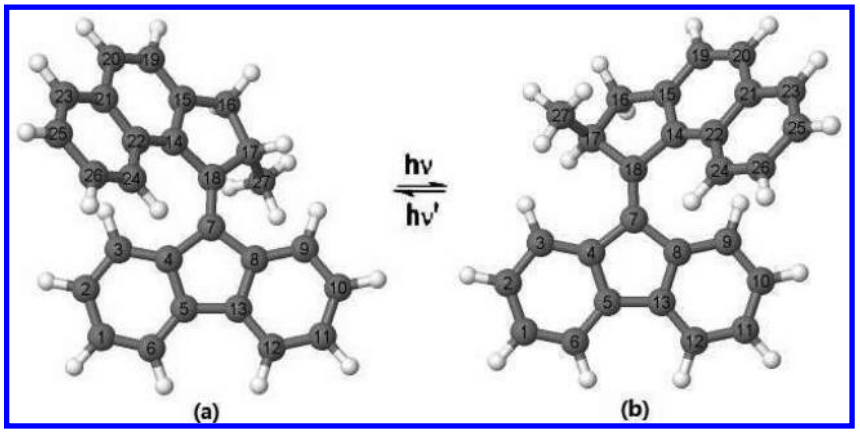

Figure 1. Optimized geometries of (a) M and (b) P structures of molecular rotary motor 9-(2-methyl-2,3-dihydro-1*H*-cyclopenta[*a*]naphthalen-1-ylidene)-9*H*-fluorene calculated at OM2/MRCI level. All carbon atoms are labeled.

semiempirical quantum-chemical calculations.[35] The working mechanism of a chiral stilbene light-driven molecular rotary motor was studied by Liu et al.[36] at the CASPT2//CASSCF level of theory. The photoisomerization reaction was described as a three-state multimode mechanism. With ab initio molecular orbital calculations, topographical features around the conical intersection of a fluorene-based light-driven molecular motor has been examined by Amatatsu.[37] Filatov et al.[38] found that, through designing the conical intersection, a molecular rotary motor can experience an effective axial rotational motion. Very recently, two new light-driven molecular rotary motors based on N-alkylated indanylidene benzopyrrole frameworks were proposed by Nikiforov et al.,[39] which are predicted to display a quantum efficiency higher than that of the currently available synthetic all-hydrocarbon motors.

In experiments, Conyard et al.[40] recently used ultrafast fluorescence up-conversion spectroscopy with a time resolution better than 50 fs to probe the earliest excited state dynamics of a molecular rotary motor, 9-(2-methyl-2,3-dihydro-1*H*-cyclopenta[*a*]naphthalen-1-ylidene)-9*H*-fluorene (as shown in Figure 1). Ultrafast fluorescence decay within 100 fs and oscillatory dynamics in this molecular rotary motor were observed. Due to the ultrafast fluorescence decay, the existence of a dark or near-dark state was suggested. Conyard et al.[41] also found that it is possible to enhance the operational efficiency of molecular rotary motors through modifying their substituents. Very recently, with transient IR vibrational fingerprints observed in experiment, Amirjalayer et al.[42] also suggested the existence of the so-called "dark" electronic excited state, which was speculated to be a charge transfer excited state.

As far as we know, there is yet no theoretical study on the ultrafast fluorescence decay in the molecular rotary motor Conyard et al.[40,41] reported. What is the mechanism of the ultrafast fluorescence decay, i.e. the existence of a "dark state", observed by Conyard et al.? Does this "dark state" influence the operational efficiency of a molecular rotary motor? In addition, Conyard et al.[41] found that the quantum yield of the reverse photoisomerization was very large. Is there also a "dark state" existence during the reverse photoisomerization process in this molecular rotary motor? To answer these questions, and to aid in a better understanding of the power stroke process in light-driven molecular rotary motors, the photoisomerization process of the molecular rotary motor should be investigated in detail.

In this study, we systematically investigated the photo-induced isomerization dynamics of the light-driven molecular rotary motor 9-(2-methyl-2,3-dihydro-1*H*-cyclopenta[*a*]-naphthalen-1-ylidene)-9*H*-fluorene by using a trajectory surface-hopping method at the OM2/MRCI level of theory. Although two S_0/S_1 minimum-energy conical intersections are obtained at the OM2/MRCI level, only one conical intersection is found to be responsible for the nonadiabatic dynamics. The existence of the "dark state" in the molecular rotary motor is confirmed through the simulated time-resolved fluorescence emission spectrum. We find that this "dark state" in the molecular rotary motor is not a new electronic state involving different electronic transitions, but the "dark region" of the initial S_1 state when trajectories move away from the Franck–Condon region.

The paper is organized as follows: In section II, we discuss the basic theoretical method and the simulation details. The results of the molecular rotary motor are presented in section III, in which the potential energy surface and time-resolved fluorescence emission spectrum are also discussed. Finally, we summarize our results and discussion in section IV.

II. COMPUTATIONAL DETAILS

All semiempirical calculations were performed with the OM2/MRCI method as implemented in the development version of the MNDO program.[43] This method can provide a reasonable compromise between computational cost and accuracy, as shown by many benchmark calculations,[44−46] and has been successfully used in previous studies of many photoinduced processes.[35,39,47−50] The required energies, gradients, and nonadiabatic couplings were calculated analytically. The self-consistent field (SCF) calculations were done in the restricted open-shell Hartree−Fock (ROHF) formalism, as it provided a better description of the excited-state wave functions. Three reference configurations including the closed-shell ground-state configurations combined with single and double excitations from the highest occupied molecular orbital (HOMO) to the the lowest unoccupied molecular orbital (LUMO) were used to generate multireference configuration interaction (MRCI) expansion.

The active space in the MRCI calculations included 10 electrons in 10 orbitals (π and π^* orbitals), which turned out to be quite robust not only for the geometry optimizations and the corresponding dynamics simulation but also the locating of conical intersections. Meanwhile, we used the π-type population (PIPOP) method[51,58] with thresholds of 0.4 to identify and track the π character orbitals and keep the π

DOI: 10.1021/acs.jpca.6b12253
J. Phys. Chem. A 2017, 121, 1240−1249

orbitals in the active space. The geometries of the ground state S_0 and the first excited state S_1 minima were optimized at the OM2/MRCI level. The optimization of the S_0/S_1 minimum-energy conical intersections (CIs) structures were located by the Lagrange−Newton[57] approach.

The photoinduced nonadiabatic dynamics of a molecular rotary motor starting from the M structure in Figure 1 was investigated by the trajectory surface-hopping simulation with Tully's fewest-switches algorithm.[52−55] The initial geometries and velocities of 207 trajectories were extracted from the Wigner distribution function of vibrational normal modes on the S_0 state.[54,56] The time step to propagate the nuclear motion was 0.1 fs, and a 100 times smaller time step was used for the electronic propagation.

The time-resolved fluorescence emission spectrum was extracted from the nonadiabatic dynamics simulation results including state energy, oscillator strengths, and current electronic state of all trajectories in our simulation. To calculate the fluorescence intensity at every moment, a time step of 10 fs was used by summing the oscillator strengths over all trajectories remaining on the excited state. In the current work, only a brief description of the calculation method is shown below. The detailed theoretical foundation can be found in the previous works of Lan et al.[58] and Jin et al.[59]

The emission intensity $I(\omega,t)^{\text{emission}}$ at time t can be calculated by

$$I(\omega, t)^{\text{emission}} \propto \omega^3 \sum_{i=1}^{N_1} f(\omega_i, t)\, \delta(\omega - \omega_i) \tag{1}$$

where $f(\omega_i,t)$ is the oscillator strength of the ith trajectory at time t and N_1 is the number of geometries staying on the S_1 excited state, since there is no emission after the hopping to the ground state.

The overall integrated emissions in the time and frequency domains are determined by

$$I(t)^{\text{emission}} = \int I(\omega, t)^{\text{emission}}\, \mathrm{d}\omega \tag{2}$$

and

$$I(\omega)^{\text{emission}} = \int I(\omega, t)^{\text{emission}}\, \mathrm{d}t \tag{3}$$

III. RESULTS AND DISCUSSION

III.A. Equilibrium Structures. Before the dynamical simulation of the M-to-P photoisomerization process, we first optimize the ground state M and P structures of this molecular rotary motor at the OM2/MRCI level. The optimized geometries are presented in Figure 1 and Table 1. For comparison, the corresponding values calculated with B3LYP/6-31G(d,p) using the Gaussian 03 software package[60] are also shown in Table 1. One can see that the results obtained with OM2/MRCI in MNDO99 are in quite good agreement with those obtained in the density-functional calculations.

As can be seen in Table 1, some twists exist around the C7═C18 double bond, and the dihedral angles of C8−C7−C18−C14 in M and P structures are −158.0 and −11.6°, respectively. Almost no pyramidalization was observed at the C7 atom in both M and P isomers. The energy of the M structure is slightly higher (2.04 kcal/mol) than that of the P conformer at the OM2/MRCI level, consistent with the 3.59 kcal/mol energy difference obtained with the B3LYP/6-31G(d,p) level. Both results confirm that the P structure is slightly more stable than the corresponding M structure.

Table 1. Optimized Geometrical Parameters of M and P Structures of the Molecular Rotary Motor, Calculated with OM2/MRCI and B3LYP/6-31G(d,p) Levels[a]

		OM2/MRCI	B3LYP/6-31G(d,p)
M	C8−C7−C18−C14	−158.0	−153.3
	C7−C18−C14−C22	26.2	27.7
	C7−C4−C8−C18	−1.6	−1.50
	C8−C7−C18	126.5	126.8
	C7−C18−C14	127.6	128.6
	C8−C7	1.48	1.48
	C7−C18	1.36	1.38
	C18−C14	1.47	1.47
P	C8−C7−C18−C14	−11.6	−14.2
	C7−C18−C14−C22	−39.8	−41.5
	C7−C4−C8−C18	−0.7	−1.8
	C8−C7−C18	127.6	128.4
	C7−C18−C14	128.1	130.1
	C8−C7	1.48	1.49
	C7−C18	1.36	1.37
	C18−C14	1.47	1.48

[a]The lengths are in angstroms; the dihedral angles and bond angles are in degrees.

The geometry of the first excited state S_1 minimum is also optimized at the OM2/MRCI level. Only one S_1 minimum is obtained, which is independent of the initial geometries P or M in optimization. The optimized geometry of S_1 minimum is presented in Figure 3a, while its geometrical parameters are listed in Table 2. The dihedral angle C8−C7−C18−C14 and pyramidalization at the C7 atom in the S_1 minimum are −108.3 and −16.8°, respectively. Thus, a significant twist around the central C7═C18 bond and an obvious pyramidalization at the C7 atom were observed at the S_1 minimum.

III.B. Nonadiabatic Photoisomerization Dynamics. Based on the vibrational normal modes of ground state M structure, the initial geometries and velocities for nonadiabatic dynamics simulations are extracted from the Wigner distribution function. Molecular dynamics simulations of a total 207 trajectories starting from the S_1 state are carried out with the OM2/MRCI method for 2000 fs. The S_1 excited state corresponds to the electron transition from HOMO to LUMO, i.e., from the bonding π to the antibonding π^* orbital of the central C═C double bond. In the 207 trajectories, 195 trajectories decay to the ground state before the end of 2000 fs, and the other 12 trajectories still stay in the S_1 excited state. In the 195 trajectories which de-excite to the S_0 state within 2000 fs, 124 trajectories experience the M-to-P photoisomerization, which means that the quantum yield of M-to-P photoisomerization of the molecular rotary motor is about 59.9%. Our calculated quantum yield is a little higher than that of experimental measurements[41] (50.0%). The quantitative difference may be due to the fact that the experiments were done using dichloromethane solutions, whereas our calculations consider the reaction in the gas phase.

The average occupation of the electronic states S_0 and S_1 as a function of simulation time is shown in Figure 2. As we can see, most fast decay events occur between 400 and 700 fs, while the further slow de-excitation lasts to the end of the simulation. The S_1 time-dependent fractional occupation is fitted by a multiexponential function, and two different decay time scales

DOI: 10.1021/acs.jpca.6b12253
J. Phys. Chem. A 2017, 121, 1240−1249

Table 2. Optimized Geometrical Parameters of the S_1 Minimum Energy Structure and Two S_0/S_1 Conical Intersections (CIs) Calculated at OM2/MRCI Level[a]

structure	C8−C7−C18−C14	C7−C18−C14−C22	C7−C4−C8−C18	C8−C7−C18	C7−C18−C14	C8−C7	C7−C18	C18−C14
S_1-min	−108.3	−1.1	−16.8	121.6	124.5	1.46	1.40	1.44
CI_1	−112.6	−2.9	−36.9	105.6	120.0	1.51	1.43	1.44
CI_2	−53.7	−15.5	34.6	101.6	136.2	1.50	1.41	1.47

[a]The lengths are in angstroms; the dihedral angles and bond angles are in degrees.

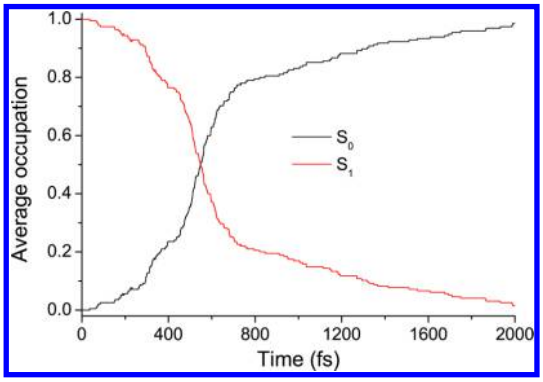

Figure 2. Average occupation of electronic states S_0 and S_1 as a function of simulation time.

(500 fs and 1.0 ps) were identified. By considering the ratio of fast and slow decay trajectories, the averaged lifetime of the S_1 excited state is estimated to be about 710 fs.

Based on available geometries at hopping events, we optimize the S_0/S_1 conical intersections (CIs) at the OM2/MRCI level. Two different minimal energy CIs, CI_1 and CI_2 in Figure 3, are obtained, which are characterized by different dihedral angles C8−C7−C18−C14 (−122.6 and −53.7°), respectively. Other geometrical parameters of these two conical intersections are listed in Table 2. It is clear that both CIs involve strong pyramidalization at the C7 atom site. Similar pyramidalization of the carbon atom at the stator−axle linkage was also observed by Kazaryan et al.[35] in another molecular rotary motor.

Although two CIs are located, CI_1 is mainly responsible for the nonadiabatic decay dynamics. Among all trajectories jumping back to the S_0 state within 2000 fs, 192 trajectories decay through the CI_1 channel, while only three trajectories de-excite through the CI_2 channel. The dominant role of CI_1 in the nonadiabatic decay mechanism can be well understood by its energy and geometry. The S_0 and S_1 potential energy surfaces and their two-dimensional contours are shown in Figure 4.

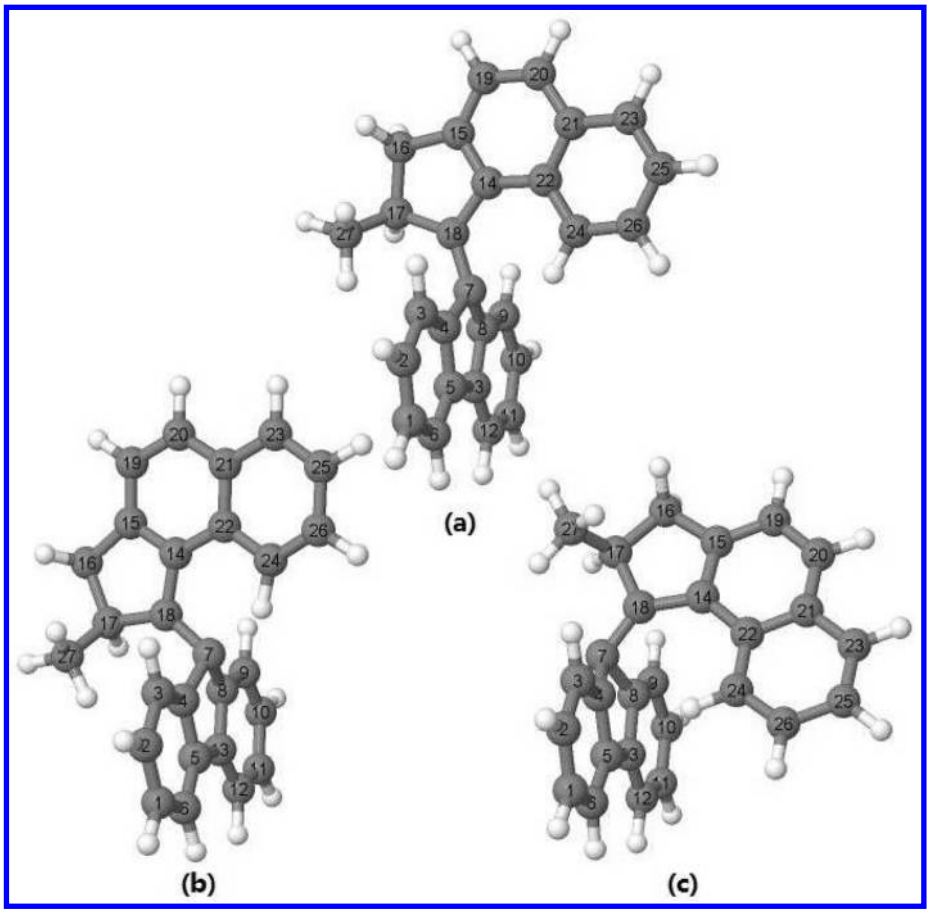

Figure 3. Optimized geometries of (a) S_1 minimum energy structure and two S_0/S_1 conical intersections (b) CI_1 and (c) CI_2 calculated with OM2/MRCI method. All carbon atoms are labeled the same as in Figure 1.

DOI: 10.1021/acs.jpca.6b12253
J. Phys. Chem. A 2017, 121, 1240−1249

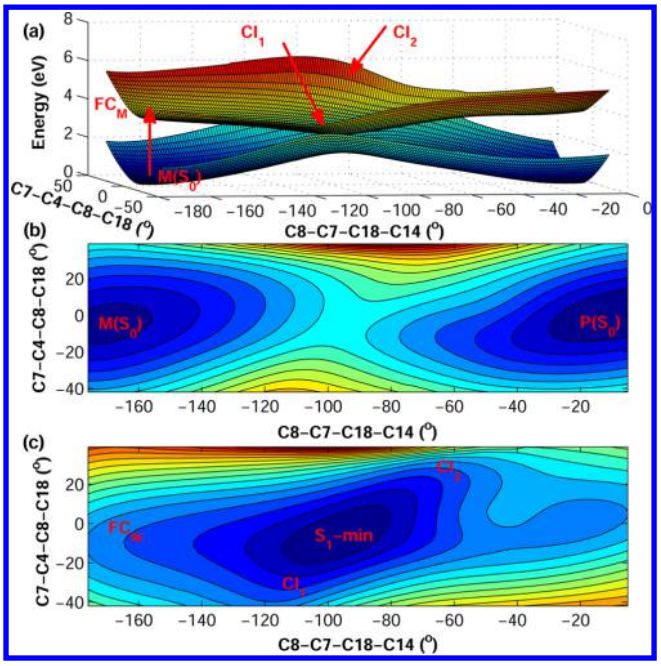

Figure 4. (a) Profiles of the S_1 (upper) and S_0 (bottom) potential energy surfaces, and two-dimensional contours of (b) S_0 and (c) S_1 potential energy surfaces calculated with OM2/MRCI as functions of two dihedral angles C8−C7−C18−C14 and C7−C4−C8−C18. The positions for the optimized structure of the S_1 minimum, the geometry of the Franck−Condon region near $M(S_0)$, and the two conical intersections CI_1 and CI_2 are also displayed.

Positions of the optimized ground state structures for M and P geometries (labeled as $M(S_0)$ and $P(S_0)$ respectively), the optimized structure of the S_1 minimum, the two S_0/S_1 conical intersections, and the geometry of the Franck−Condon region near $M(S_0)$ (labeled as FC_M) are displayed in Figure 4.

Energies of different geometries on the S_0 and S_1 states obtained at the OM2/MRCI level are listed in Table 3. All values are given relative to the optimized ground state of the P conformer. As can be seen in Figure 4c and Table 3, the total energy of CI_1 lies 6.99 kcal/mol lower than that of the corresponding CI_2 structure, the nonadiabatic decay route from FC_M to CI_1 is barrierless with steep gradients in the S_1 potential energy surface, and the other route from FC_M to CI_2 is very flat in the S_1 potential energy surface (with only little gradients). Together with that CI_1 is closer to FC_M than CI_2, less torsional motion is required from FC_M to CI_1. In a word, decay is much more accessible through the CI_1 channel than through the CI_2 channel, consistent with our trajectory simulation results.

Table 3. Energies of Different Geometries on S_0 and S_1 States Obtained at OM2/MRCI Level (in kcal/mol);[a] Energy Differences between S_0 and S_1 (ΔE, i.e. Transition Energy) and Oscillator Strength f of $S_0 \rightarrow S_1$ Transition at Different Geometries

	M	P	S_1-min	CI_1	CI_2
S_0	2.04	0	38.64	61.06	68.05
S_1	81.52	85.07	57.42	61.06	68.05
ΔE	79.48	85.07	18.78	0.00	0.00
f	0.85	0.90	0.00	0.00	0.00

[a]All values are given relative to the optimized ground state of P conformer.

We should emphasize that, although two decay time constants are gotten through the above fitting procedure for Figure 2, it is not contradictory to the fact that only the single channel via CI_1 is responsible for the nonadiabatic decay dynamics in this molecular rotary motor. Some trajectories may pass by the S_1-min region, and then directly decay to the ground state through the conical intersection CI_1 within a short time (red lines shown in Figure 5). The other trajectories, on the other hand, may stay near the S_1-min region and the upper adiabatic surface for a longer time duration and then decay via CI_1 (blue lines displayed in Figure 5). The different behaviors of trajectories can well explain the origin of two decay time constants. Thus, instead of the existence of two different reaction channels, the multiple decay constants come from the different behaviors of trajectory propagation during their accessing the CI_1.

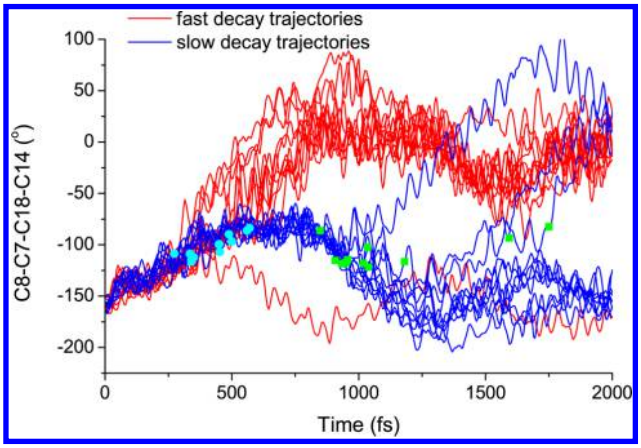

Figure 5. A few of representative trajectories for nonadiabatic decay dynamics of molecular rotary motor. Red lines represent fast decay trajectories with cyan circles indicating their hopping times, while blue lines represent slow decay trajectories with green squares showing hopping times.

In order to deeply understand the isomerization process, we now turn to a detailed discussion of the isomerization process in a single representative trajectory which experiences the M-to-P photoisomerization via the CI_1 channel.

When the M structure of the molecular rotary motor is pumped to the S_1 excited state, as can be seen in Figure 6a, the molecular rotary motor stays at the excited state until it jumps back to the ground state at 559.3 fs. After the excitation, as shown in Figure 7a, the central C7−C18 bond connecting the corresponding rotor part and the stator part is weakened, increasing from its optimized ground state length of 1.36 Å to 1.47 Å, vibrating around 1.42 Å until 560 fs, and then returning to 1.37 Å quickly after the de-excitation. That is, the excitation from the bonding π orbital of the central C═C double bond to the antibonding π^* orbital reduces its double bond character obviously. The two neighboring C−C bonds C7−C8 and C14−C18 connected with the central C7−C18, on the other hand, are shortened from 1.48 to 1.43 Å after the excitation, and also return to their initial values in ground state after the de-excitation.

Time evolution of the three dihedral angles C8−C7−C18−C14, C7−C18−C14−C22, and C7−C4−C8−C18 are presented in Figure 8. After excitation, the central C8−C7−C18−C14 dihedral angle increases from its optimized ground state value of −158° gradually, reaches −91.3° at 559.3 fs when

DOI: 10.1021/acs.jpca.6b12253
J. Phys. Chem. A 2017, 121, 1240−1249

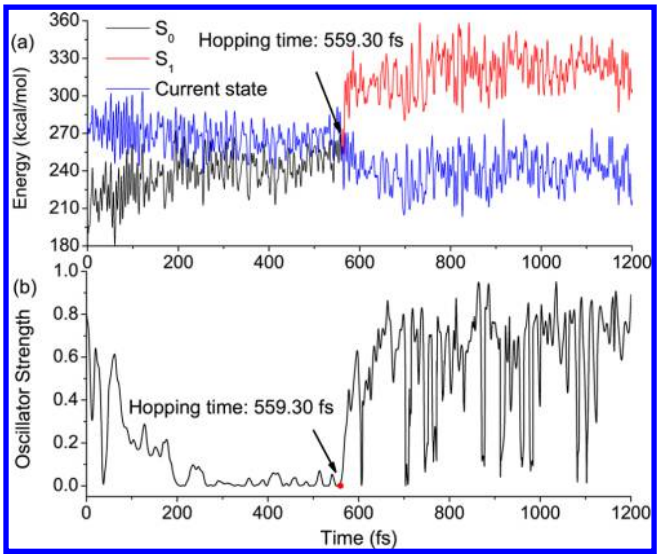

Figure 6. Time dependence of (a) potential energies of S_0 and S_1 states and (b) $S_0 \rightarrow S_1$ oscillator strength in a typical single representative trajectory. The time of hopping event is also displayed.

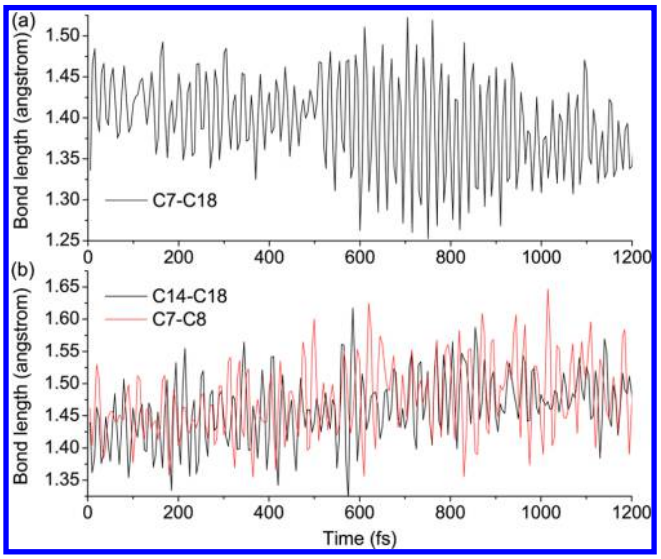

Figure 7. Time dependence of (a) central C═C bond length and (b) bond lengths of two connected C−C single bonds.

nonadiabatic decay occurs, and then increases dramatically to −11.6° to form the P structure after about 700 fs, which can be a demonstration of the completion of the M-to-P isomerization process. Another dihedral angle, C7−C18−C14−C22, decreases from about 20° to −40° after the excitation, and then vibrates around this value until the end of our simulation. The dihedral angle C7−C4−C8−C18, characterizing the pyramidalization at the C7 atom, decreases from −1.6° at time zero to −24.9° at 559.3 fs, and then goes to its optimized ground state value of −0.7° in the P structure after 700 fs.

Both optimized geometries of conical intersections presented in Figure 3 and the time dependence of geometrical parameters shown in Figure 8 verify that, after the excitation, the dynamical process of nonadiabatic decay is followed by twisting about the central C═C double bond and the pyramidalization of the C atom at the stator−axle linkage.

III.C. Time-Dependent Fluorescence and Dark State. To aid in a better understanding of the fluorescence emission

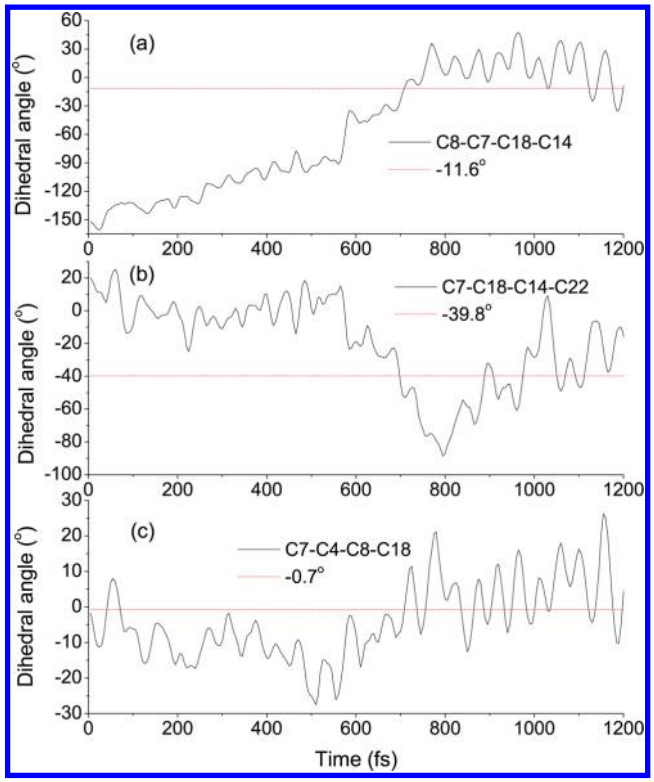

Figure 8. Time dependence of (a) central dihedral angle C8−C7−C18−C14, (b) side dihedral angle C7−C18−C14−C22, and (c) pyramid dihedral angle C7−C4−C8−C18 in a typical single representative trajectory.

spectrum observed by Conyard et al.[40,41] theoretically, the time-resolved fluorescence emission spectrum during the M-to-P photoisomerization process in the molecular rotary motor is calculated based on the 207 trajectories in our simulations.

The two-dimensional contour of the fluorescence emission intensity in the time and frequency domain is presented in Figure 9a. The calculated fluorescence emission spectrum reflects that the ultrafast quenching of fluorescence emission occurs before 150 fs, accompanied by a red shift of the wavenumber of the emission photon. In addition, several temporal evolutions of the wavelength-resolved fluorescence emission spectrum at different times ranging from 15 to 150 fs are plotted in Figure 9b in different colors. As we can see, the central wavenumber of the emission spectrum at 15 fs is about 2.4×10^4 cm^{-1}. But the central wavenumber of the emission spectrum at 150 fs is about 1.55×10^4 cm^{-1}, with an intensity much weaker (about one-tenth) than that at 15 fs. There is no doubt that the feature of Figure 9b is more evidence for the red shift and quenching of the fluorescence emission spectrum.

Since the lifetime of the fluorescence emission is about 150 fs, much shorter than that of the S_1 excited state (about 710 fs), the dark state must exist during the M-to-P photoisomerization process of the molecular rotary motor.

To "watch" the dark state more directly, time dependence of the oscillator strength of the $S_0 \rightarrow S_1$ transition in the typical single representative trajectory is shown in Figure 6b. As we can see, the oscillator strength decreases gradually before 200 fs. The energy difference between the S_0 and S_1 states, as shown in Figure 6a, also decreases gradually before 200 fs. That is why we can see the red shift of the fluorescence emission spectrum in Figure 9. Afterward, the oscillator strength is close to zero for

DOI: 10.1021/acs.jpca.6b12253
J. Phys. Chem. A 2017, 121, 1240−1249

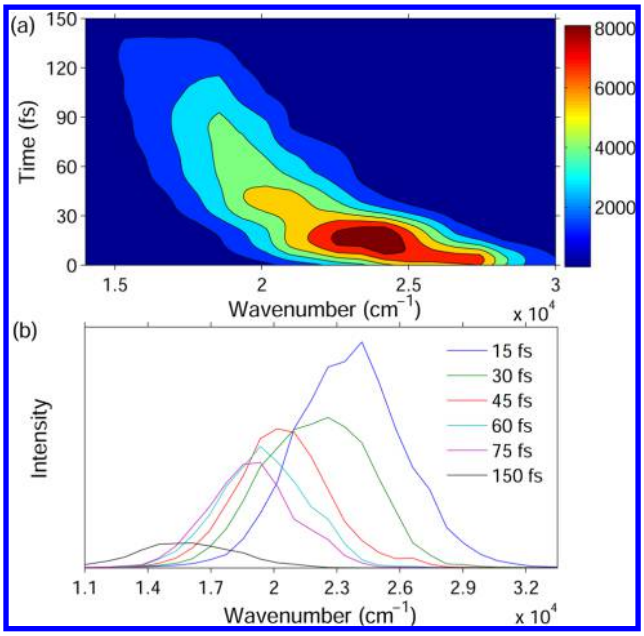

Figure 9. Time-dependent fluorescence emission spectrum of molecular rotary motor. (a) Two-dimensional contour of emission intensity with respect to simulation time and wavenumber of photon. (b) Wavelength-resolved fluorescence emission spectrum at different times.

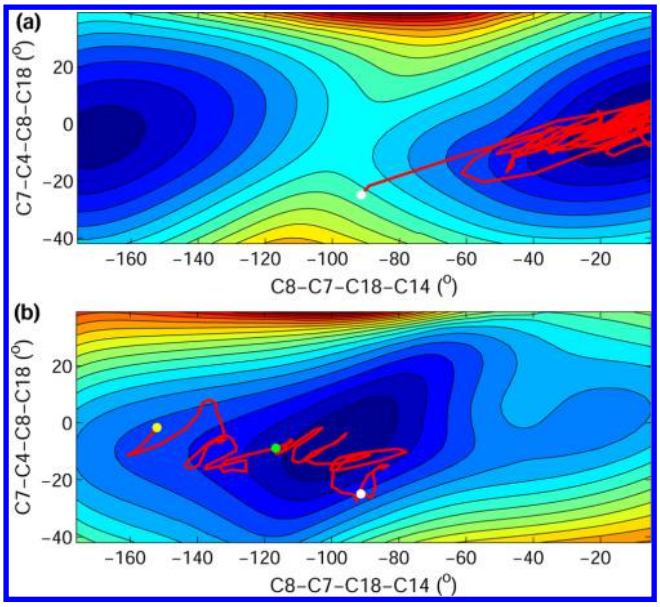

Figure 10. Trajectory of typical single representative simulation (as presented in Figures 6–8) shown in two-dimensional contours of the (a) S_0 and (b) S_1 potential energy surfaces as functions of dihedral angles C8–C7–C18–C14 and C7–C4–C8–C18. The yellow dot represents the start of the trajectory, while the green dot is the starting point (about 200 fs) of the "dark state" until arriving at the white dot where the molecular rotary motor de-excites to the ground state at 559.30 fs.

a long time although the trajectory is still in the excited state. This indicates that quenching of the emission should take place before the trajectory jumps back to the ground state. In other words, it is possible to assume that the molecular rotary motor stays at the dark state before the nonadiabatic decay takes place.

The energy differences between the S_0 and S_1 states, i.e. transition energy, and the oscillator strength of the $S_0 \rightarrow S_1$ transition at different geometries are listed in Table 3. As we can see, the transition energy at the S_1 minimum (18.78 kcal/mol) is much smaller than that at the Franck–Condon region near the M structure (79.48 kcal/mol). The oscillator strength of the $S_0 \rightarrow S_1$ transition at the M conformer is quite large, while those at the S_1 minimum and both CI structures are all zero. That is, there is no fluorescence emission near the S_1 minimum and both CI regions.

Furthermore, to establish a fundamental understanding of the relationship between molecular geometry and dark state, the representative trajectory discussed above is shown in the two-dimensional contours of the S_0 and S_1 potential energy surfaces as functions of dihedral angles C8–C7–C18–C14 and C7–C4–C8–C18. As displayed in Figure 10, the yellow dot represents the start of the trajectory, while the green dot is the starting point of the "dark state" (about 200 fs) until arriving at the white dot where the molecular rotary motor de-excites to the ground state at 559.30 fs. It is obvious that all geometries of the "dark state" locate close to the S_1 minimum energy structure in this trajectory. After the de-excitation, the molecular rotary motor arrives at its stable P structure very quickly. Since the locations of both conical intersections are far from that of the S_1 minimum energy structure, as can be seen in Figure 4c, and the oscillator strength of the $S_0 \rightarrow S_1$ transition around the S_1 minimum energy structure is nearly zero, this molecular rotary motor stays on the "dark state" for a long time.

We should emphasize that, as discussed above, the "dark state" in this molecular rotary motor is not a different electronic state, but still the S_1 excited state while the oscillator strength of the $S_0 \rightarrow S_1$ transition vanishes. A "dark region" near the S_1 minimum and two conical intersections exists in the S_1 excited state potential energy surface. That is why we observed quenching of fluorescence emission in the excited state dynamics of the molecular rotary motor.

In their work, Amirjalayer et al.[42] attributed the ultrafast decay of emission to the involvement of the additional "dark" electronic excited state that was speculated to be a charge transfer excited state. Based on the theoretical calculations with single reference time-dependent DFT and SCS-CC2 methods, they assumed that this intruded state is characterized by the HOMO-1 → LUMO transition, different from the S_1 character (HOMO → LUMO transition) at the S_0 geometry. Based on this idea, they also suggested that nonadiabatic dynamics of the current motor is not simply governed by the ethylene-type decay involving double bond twisting motion and pyramidalization at one C site.[61,62] However, our dynamics simulation at the OM2/MRCI level proposed an alternative mechanism.

At the OM2/MRCI level, the S_1 state at the S_0 minimum is characterized by the HOMO → LUMO transition. The frontier orbitals of this molecular rotary motor at several critical geometries are displayed in Figure 11. At the S_1 minimum or CI geometry, two relevant configurations in the MRCI expansion are still closed-shell and open-shell singlet in the basis of two frontier orbitals. Although it is clear that the orbital localization is observed at these two geometries, two frontier orbitals can essentially be treated as the linear combination of HOMO and LUMO at the S_0 minimum energy geometry. Thus, no completed new electronic character is involved in the dynamics from S_0 to CI. This observation can be further proven by examining the energies and electronic characters of higher excited states. The S_2 state is always characterized by the HOMO-1 → LUMO transition and lies much higher (at least

DOI: 10.1021/acs.jpca.6b12253
J. Phys. Chem. A 2017, 121, 1240–1249

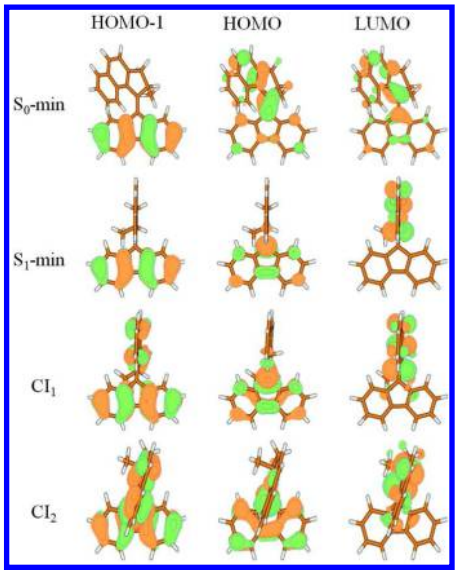

Figure 11. Molecular orbitals of the molecular rotary motor at several critical geometries: S_0-min, S_1-min, and two S_0/S_1 conical intersections.

0.6 eV higher than those of S_1 states) at critical geometries (S_0-min, S_1-min, and CI). Thus, the S_2 state is not involved in the nonadiabatic dynamics at the OM2/MRCI level.

Certainly, we should not neglect the localization effects of two frontier orbitals when the central double bond starts to twist. This feature widely exists in many double bond twisting systems.[61−66] As a result of it, the $S_0 \rightarrow S_1$ transition becomes essentially dark and this explains the "dark" feature in experiments. Although the S_1 state may possess ionic character, it is not attributed to the appearance of an intruded state with completed novel electronic transitions. Thus, we prefer to suggest that the involved electronic character of S_1 remains during the trajectory propagation. The appearance of the "dark" feature in the experimental observation is relevant to the fact that trajectories access the region of the S_1 state with vanishing oscillator strength.

IV. CONCLUSIONS

With trajectory surface-hopping dynamics based on the OM2/MRCI level, M-to-P photoisomerization dynamics of the light-driven molecular rotary motor 9-(2-methyl-2,3-dihydro-1*H*-cyclopenta[*a*]naphthalen-1-ylidene)-9*H*-fluorene is investigated in detail. Based on 207 trajectories, two different decay time scales (500 fs and 1.0 ps) were identified for the lifetime of the S_1 state. By weighting the contributions of fast and slow decay trajectories, the averaged S_1 lifetime is about 710 fs. After the $S_0 \rightarrow S_1$ excitation, the dynamical process of electronic de-excitation is followed by twisting about the central C═C double bond and the motion of pyramidalization at the carbon atom of the stator−axle linkage. Although two S_0/S_1 minimum-energy conical intersections are obtained at the OM2/MRCI level, only one conical intersection is found to be responsible for the nonadiabatic dynamics.

The existence of a "dark state" in the excited-state dynamics of this molecular rotary motor is confirmed through the simulated time-resolved fluorescence emission spectrum, in which the fluorescence emission nearly disappears after 150 fs, although most of molecular rotary motors are still in the S_1 excited state. Red shift of the fluorescence emission spectrum is also observed in our calculation. Since the locations of the conical intersections are far from that of the S_1 minimum energy structure, and the oscillator strength of $S_0 \rightarrow S_1$ transition around the S_1 minimum energy structure is nearly zero, this molecular rotary motor stays at the dark state for a long time. Proper structural modification could vary the location of CIs, and make the dark state lifetime much shorter, even lead to no existence of the dark state, which may increase the photochemical efficiency of the molecular rotary motor considerably. This opens a route to design new molecular rotary motors with high operational efficiency.

AUTHOR INFORMATION

Corresponding Authors

*Tel.: +86-29-82663339. E-mail: jiangcw@mail.xjtu.edu.cn (C.J.).

*Tel.: +86-532-80662630. E-mail: lanzg@qibebt.ac.cn (Z.L.).

ORCID

Chenwei Jiang: 0000-0002-3536-3245

Notes

The authors declare no competing financial interest.

ACKNOWLEDGMENTS

This work was supported by the Natural Science Foundation of China (Grants 21203144, 21673266, 21543008, 11534008, and 11504288), the Doctoral Fund of Ministry of Education of China (Grant 20120201120056), the Fundamental Research Funds for the Central Universities (xjj2016053), and the HPC Platform in Xi'an Jiaotong University. C.J. thanks the China Scholarship Council for financial support. Z.L. thanks the Distinguished Young Scholars (JQ201504) from the Natural Science Foundation of Shandong Province for support.

REFERENCES

(1) Feringa, B. L. In Control of Motion: From Molecular Switches to Molecular Motors. *Acc. Chem. Res.* **2001**, *34*, 504−513.

(2) Kottas, G. S.; Clarke, L. I.; Horinek, D.; Michl, J. Artificial Molecular Rotors. *Chem. Rev.* **2005**, *105*, 1281−1376.

(3) Erbas-Cakmak, S.; Leigh, D. A.; McTernan, C. T.; Nussbaumer, A. L. Artificial Molecular Machines. *Chem. Rev.* **2015**, *115*, 10081−10206.

(4) Seldenthuis, J. S.; Prins, F.; Thijssen, J. M.; vander Zant, H. S. J. An All-electric Single-molecule Motor. *ACS Nano* **2010**, *4*, 6681−6686.

(5) Neumann, J.; Gottschalk, K. E.; Astumian, R. D. Driving and Controlling Molecular Surface Rotors with a Terahertz Electric Field. *ACS Nano* **2012**, *6*, 5242−5248.

(6) Kudernac, T.; Ruangsupapichat, N.; Parschau, M.; Macia, B.; Katsonis, N.; Harutyunyan, S. R.; Ernst, K.-H.; Feringa, B. L. Electrically Driven Directional Motion of a Four-wheeled Molecule on a Metal Surface. *Nature* **2011**, *479*, 208−211.

(7) Kelly, T. R.; Cai, X.; Damkaci, F.; Panicker, S. B.; Tu, B.; Bushell, S. M.; Cornella, I.; Piggott, M. J.; Salives, R.; Cavero, M.; Zhao, Y.; Jasmin, S. Progress toward a Rationally Designed, Chemically Powered Rotary Molecular Motor. *J. Am. Chem. Soc.* **2007**, *129*, 376−386.

(8) Kelly, T. R.; De Silva, H.; Silva, R. A. Unidirectional Rotary Motion in a Molecular System. *Nature* **1999**, *401*, 150−152.

(9) Astumian, R. D. Thermodynamics and Kinetics of a Brownian Motor. *Science* **1997**, *276*, 917−922.

(10) Astumian, R. D.; Derenyi, I. A Chemically Reversible Brownian Motor: Application to Kinesin and Ncd. *Biophys. J.* **1999**, *77*, 993−1002.

(11) Balzani, V.; Credi, A.; Venturi, M. Light Powered Molecular Machines. *Chem. Soc. Rev.* **2009**, *38*, 1542−1550.

DOI: 10.1021/acs.jpca.6b12253
J. Phys. Chem. A 2017, 121, 1240−1249

(12) Pollard, M. M.; Lubomska, M.; Rudolf, P.; Feringa, B. L. Controlled Rotary Motion in a Monolayer of Molecular Motors. *Angew. Chem., Int. Ed.* **2007**, *46*, 1278−1280.
(13) London, G.; Carroll, G. T.; Fernandez Landaluce, T.; Pollard, M. M.; Rudolf, P.; Feringa, B. L. Light-driven Altitudinal Molecular Motors on Surfaces. *Chem. Commun.* **2009**, *91*, 1712−1714.
(14) Browne, W. R.; Feringa, B. L. Light Switching of Molecules on Surfaces. *Annu. Rev. Phys. Chem.* **2009**, *60*, 407−428.
(15) London, G.; Chen, K. Y.; Carroll, G. T.; Feringa, B. L. Towards Dynamic Control of Wettability by Using Functionalized Altitudinal Molecular Motors on Solid Surfaces. *Chem. - Eur. J.* **2013**, *19*, 10690−10697.
(16) Ogino, S.; Kawamoto, M.; Okano, K.; Yamashita, T. J. Effect of Temperature on the Surface Relief Grating Formation caused by Rotation of Light-driven Molecular Motor. *J. Photopolym. Sci. Technol.* **2013**, *26*, 563−566.
(17) Wang, J.; Feringa, B. L. Dynamic Control of Chiral Space in a Catalytic Asymmetric Reaction Using a Molecular Motor. *Science* **2011**, *331*, 1429−1432.
(18) Bauer, J.; Hou, L. L.; Kistemaker, J. C. M.; Feringa, B. L. Tuning the Rotation Rate of Light-Driven Molecular Motors. *J. Org. Chem.* **2014**, *79*, 4446−4455.
(19) Browne, W. R.; Feringa, B. L. Making Molecular Machines Work. *Nat. Nanotechnol.* **2006**, *1*, 25−35.
(20) Feringa, B. L. The Art of Building Small: From Molecular Switches to Molecular Motors. *J. Org. Chem.* **2007**, *72*, 6635−6652.
(21) Koumura, N.; Zijlstra, R. W. J.; van Delden, R. A.; Harada, N.; Feringa, B. L. Light-driven Monodirectional Molecular Rotor. *Nature* **1999**, *401*, 152−155.
(22) Vicario, J.; Meetsma, A.; Feringa, B. L. Controlling the Speed of Rotation in Molecular Motors. Dramatic Acceleration of the Rotary Motion by Structural Modification. *Chem. Commun.* **2005**, *116*, 5910−5912.
(23) Vicario, J.; Walko, M.; Meetsma, A.; Feringa, B. L. Fine Tuning of the Rotary Motion by Structural Modification in Light-Driven Unidirectional Molecular Motors. *J. Am. Chem. Soc.* **2006**, *128*, 5127−5135.
(24) Wezenberg, S. J.; Chen, K.-Y.; Feringa, B. L. Visible-Light-Driven Photoisomerization and Increased Rotation Speed of a Molecular Motor Acting as a Ligand in a Ruthenium(II) Complex. *Angew. Chem., Int. Ed.* **2015**, *54*, 11457−11461.
(25) Faulkner, A.; van Leeuwen, T.; Feringa, B. L.; Wezenberg, S. J. Allosteric Regulation of the Rotational Speed in a Light-Driven Molecular Motor. *J. Am. Chem. Soc.* **2016**, *138*, 13597−13603.
(26) Pollard, M. M.; Klok, M.; Pijper, D.; Feringa, B. L. Rate Acceleration of Light-Driven Rotary Molecular Motors. *Adv. Funct. Mater.* **2007**, *17*, 718−729.
(27) Klok, M.; Boyle, N.; Pryce, M. T.; Meetsma, A.; Browne, W. R.; Feringa, B. L. MHz Unidirectional Rotation of Molecular Rotary Motors. *J. Am. Chem. Soc.* **2008**, *130*, 10484−10485.
(28) Greb, L.; Lehn, J. M. Light-Driven Molecular Motors: Imines as Four-Step or Two-Step Unidirectional Rotors. *J. Am. Chem. Soc.* **2014**, *136*, 13114−13117.
(29) García-Iriepa, C.; Marazzi, M.; Zapata, F.; Valentini, A.; Sampedro, D.; Frutos, L. M. Chiral Hydrogen Bond Environment Providing Unidirectional Rotation in Photoactive Molecular Motors. *J. Phys. Chem. Lett.* **2013**, *4*, 1389−1396.
(30) Fang, C.; Oruganti, B.; Durbeej, B. Computational Study of the Working Mechanism and Rate Acceleration of Overcrowded Alkene-based Light-driven Rotary Molecular Motors. *RSC Adv.* **2014**, *4*, 10240−10251.
(31) Kazaryan, A.; Filatov, M. Density Functional Study of the Ground and Excited State Potential Energy Surfaces of a Light-Driven Rotary Molecular Motor (3R,3R)-(P,P)-trans-1,1,2,2,3,3,4,4-Octahydro-3,3-dimethyl-4,4-biphenanthrylidene. *J. Phys. Chem. A* **2009**, *113*, 11630−11634.
(32) Oruganti, B.; Wang, J.; Durbeej, B. Computational Insight to Improve the Thermal Isomerization Performance of Overcrowded Alkene-Based Molecular Motors Through Structural Redesign. *ChemPhysChem* **2016**, *17*, 3399−3408.
(33) Oruganti, B.; Fang, C. F.; Durbeej, B. Computational Design of Faster Rotaing Second-generation Light-driven Molecular Motors by Control of Steric Effects. *Phys. Chem. Chem. Phys.* **2015**, *17*, 21740−21751.
(34) Kazaryan, A.; Kistemaker, J. C. M.; Schafer, L. V.; Browne, W. R.; Feringa, B. L.; Filatov, M. Understanding the Dynamics Behind the Photoisomerization of a Light-Driven Fluorene Molecular Rotary Motor. *J. Phys. Chem. A* **2010**, *114*, 5058−5067.
(35) Kazaryan, A.; Lan, Z.; Schafer, L. V.; Thiel, W.; Filatov, M. Surface Hopping Excited-State Dynamics Study of the Photoisomerization of a Light-Driven Fluorene Molecular Rotary Motor. *J. Chem. Theory Comput.* **2011**, *7*, 2189−2199.
(36) Liu, F.; Morokuma, K. Computational Study on the Working Mechanism of a Stilbene Light-Driven Molecular Rotary Motor: Sloped Minimal Energy Path and Unidirectional Nonadiabatic Photoisomerization. *J. Am. Chem. Soc.* **2012**, *134*, 4864−4876.
(37) Amatatsu, Y. Theoretical Study of Topographical Features around the Conical Intersections of Fluorene-Based Light-Driven Molecular Rotary Motor. *J. Phys. Chem. A* **2013**, *117*, 3689−366.
(38) Filatov, M.; Olivucci, M. Designing Conical Intersections for Light-Driven Single Molecule Rotary Motors: From Precessional to Axial Motion. *J. Org. Chem.* **2014**, *79*, 3587−3600.
(39) Nikiforov, A.; Gamez, J. A.; Thiel, W.; Filatov, M. Computational Design of a Family of Light-Driven Rotary Molecular Motors with Improved Quantum Efficiency. *J. Phys. Chem. Lett.* **2016**, *7*, 105−110.
(40) Conyard, J.; Addison, K.; Heisler, I. A.; Cnossen, A.; Browne, W. R.; Feringa, B. L.; Meech, S. R. Ultrafast Dynamics in the Power Stroke of a Molecular Rotary Motor. *Nat. Chem.* **2012**, *4*, 547−551.
(41) Conyard, J.; Cnossen, A.; Browne, W. R.; Feringa, B. L.; Meech, S. R. Chemically Optimizing Operational Efficiency of Molecular Rotary Motors. *J. Am. Chem. Soc.* **2014**, *136*, 9692−9700.
(42) Amirjalayer, S.; Cnossen, A.; Browne, W. R.; Feringa, B. L.; Buma, W. J.; Woutersen, S. Direct Observation of a Dark State in the Photocycle of a Light-Driven Molecular Motor. *J. Phys. Chem. A* **2016**, *120*, 8606−8612.
(43) Thiel, W. *MNDO Program*, version 6.1; Max-Planck-Institut fur Kohlenforschung: Mulheim, Germany, 2007.
(44) Weber, W.; Thiel, W. Orthogonalization Corrections for Semiempirical Methods. *Theor. Chem. Acc.* **2000**, *103*, 495−506.
(45) Otte, N.; Scholten, M.; Thiel, W. Looking at Self-Consistent-Charge Density Functional Tight Binding from a Semiempirical Perspective. *J. Phys. Chem. A* **2007**, *111*, 5751−5755.
(46) Zhuang, X.; Wang, J.; Lan, Z. Photoinduced Nonadiabatic Decay and Dissociation Dynamics of Dimethylnitramine. *J. Phys. Chem. A* **2013**, *117*, 4785−4793.
(47) Heggen, B.; Lan, Z.; Thiel, W. Nonadiabatic Decay Dynamics of 9H-guanine in Aqueous Solution. *Phys. Chem. Chem. Phys.* **2012**, *14*, 8137−8146.
(48) Weingart, O.; Lan, Z.; Koslowski, A.; Thiel, W. Chiral Pathways and Periodic Decay in cis-Azobenzene Photodynamics. *J. Phys. Chem. Lett.* **2011**, *2*, 1506−1509.
(49) Xia, S.; Xie, B.; Fang, Q.; Cui, G.; Thiel, W. Excited-state Intramolecular Proton Transfer to Carbon Atoms: Nonadiabatic Surface-hopping Dynamics Simulations. *Phys. Chem. Chem. Phys.* **2015**, *17*, 9687−9697.
(50) Wang, Y.; Liu, X.; Cui, G.; Fang, W.; Thiel, W. Photoisomerization of Arylazopyrazole Photoswitches: Stereospecific Excited-State Relaxation. *Angew. Chem., Int. Ed.* **2016**, *55*, 14009−14013.
(51) Keal, T. W.; Wanko, M.; Thiel, W. Assessment of Semiempirical Methods for the Photoisomerisation of a Protonated Schiff Base. *Theor. Chem. Acc.* **2009**, *123*, 145−156.
(52) Tully, J. C. Molecular Dynamics with Electronic Transitions. *J. Chem. Phys.* **1990**, *93*, 1061−1071.

DOI: 10.1021/acs.jpca.6b12253
J. Phys. Chem. A 2017, 121, 1240−1249

(53) Hammes-Schiffer, S.; Tully, J. C. Proton Transfer in Solution: Molecular Dynamics with Quantum Transitions. *J. Chem. Phys.* **1994**, *101*, 4657−4667.
(54) Barbatti, M.; Granucci, G.; Persico, M.; Ruckenbauer, M.; Vazdar, M.; Eckert-Maksic, M.; Lischka, H. J. The On-the-fly Surface-hopping Program System NEWTON-X: Application to Ab Initio Simulation of the Nonadiabatic Photodynamics of Benchmark Systems. *J. Photochem. Photobiol., A* **2007**, *190*, 228−240.
(55) Fabiano, E.; Groenhof, G.; Thiel, W. Approximate Switching Algorithms for Trajectory Surface Hopping. *Chem. Phys.* **2008**, *351*, 111−116.
(56) Wigner, E. On the Quantum Correction for Thermodynamic Equilibrium. *Phys. Rev.* **1932**, *40*, 749−759.
(57) Keal, T. W.; Koslowski, A.; Thiel, W. Comparison of Algorithms for Conical Intersection Optimization Using Semiempirical Methods. *Theor. Chem. Acc.* **2007**, *118*, 837−844.
(58) Lan, Z.; Lu, Y.; Weingart, O.; Thiel, W. Nonadiabatic Decay Dynamics of a Benzylidene Malononitrile. *J. Phys. Chem. A* **2012**, *116*, 1510−1518.
(59) Jin, H.; Liang, M.; Arzhantsev, S.; Li, X.; Maroncelli, M. Photophysical Characterization of Benzylidene Malononitriles as Probes of Solvent Friction. *J. Phys. Chem. B* **2010**, *114*, 7565−7578.
(60) Frisch, M. J.; Trucks, G. W.; Schlegel, H. B.; Scuseria, G. E.; Robb, M. A.; Cheeseman, J. R.; Montgomery, J. A., Jr.; Vreven, T.; Kudin, K. N.; Burant, J. C.; et al. *Gaussian 03*, revision C.02; Gaussian, Inc.: Wallingford, CT, 2004.
(61) Salem, L. The Sudden Polarization Effect and its Possible Role in Vision. *Acc. Chem. Res.* **1979**, *12*, 87−92.
(62) Ben-Nun, M.; Martínez, T. J. Photodynamics of Ethylene: Ab Initio Studies of Conical Intersections. *Chem. Phys.* **2000**, *259*, 237−248.
(63) Levine, B. G.; Martínez, T. J. Isomerization Through Conical Intersections. *Annu. Rev. Phys. Chem.* **2007**, *58*, 613−634.
(64) Sobolewski, A. L.; Domcke, W.; Hättig, C. Photophysics of Organic Photostabilizers. Ab Initio Study of the Excited-State Deactivation Mechanisms of 2-(2′-Hydroxyphenyl)benzotriazole. *J. Phys. Chem. A* **2006**, *110*, 6301−6306.
(65) Barbatti, M.; Ruckenbauer, M.; Szymczak, J. J.; Aquino, A. J. A.; Lischka, H. Nonadiabatic Excited-state Dynamics of Polar π-systems and Related Model Compounds of Biological Relevance. *Phys. Chem. Chem. Phys.* **2008**, *10*, 482−494.
(66) Hu, D.; Huang, J.; Xie, Y.; Yue, L.; Zhuang, X.; Lan, Z. Nonadiabatic Dynamics and Photoisomerization of Biomimetic Photoswitches. *Chem. Phys.* **2015**, *463*, 95−105.

DOI: 10.1021/acs.jpca.6b12253
J. Phys. Chem. A 2017, 121, 1240−1249